Applied Physics Express **7**, 101801 (2014)
http://dx.doi.org/**10.7567/APEX.7.101801**

Highly flexible titanium dioxide-based resistive switching memory with simple fabrication

Seung-Won Yeom[1], Suk Won Park[2], In-sung Jung[3], Minseok Kim[1],
Hyeon Jun Ha[1], Joon Hyung Shim[2], and Byeong-kwon Ju[1]*

[1]*Display and Nanosystem Laboratory, College of Engineering, Korea University, Seoul 139-713, Republic of Korea*
[2]*Renewable Energy System Laboratory, College of Mechanical Engineering, Korea University, Seoul 136-701, Republic of Korea*
[3]*New and Renewable Energy Material Development Center (NewREC), Jeonbuk National University, Jeonju 567, Republic of Korea*
E-mail: bkju@korea.ac.kr

Received August 20, 2014; accepted September 11, 2014; published online October 3, 2014

We demonstrate a flexible resistive switching random access memory (ReRAM), which is a promising next-generation memory on a flexible substrate. The proposed method enables us to fabricate an $Al/TiO_2/Al$ structure on a polyimide substrate, which has highly flexible and durable characteristics, rather than a Si-based substrate by a simple fabrication process. To understand the role of oxygen vacancies in TiO_2, our devices was analyzed by X-ray photoelectron spectroscopy (XPS) and XPS depth profile analyses. Moreover, severe bending of the device did not affect the memory performance owing to its small channel length and the high ductility of the electrode. The results presented here can provide a new approach to the fabrication of nonvolatile memories for flexible electronic devices. © 2014 The Japan Society of Applied Physics

Many flexible electronics, such as wearable devices, have attracted significant attention owing to their advantages of portability, light weight, and human-friendly interfaces over conventional bulk silicon technology for electronic paper, transistors for liquid crystal displays, sensors, solar cells, and organic light-emitting diodes.[1–3] On the basis of these state-of-the-art trends, the need for a flexible memory to support these flexible electronic devices is increasing, similar to the role of flash memories in solid-state electronics today. A flexible memory is a vital component of electronic systems for data processing, storage, and communication, and is thus a key element in the realization of such flexible electronic systems.[4]

Regarding memories, the resistance switching phenomenon in simple metal/oxide/metal sandwich structures has been the subject of concentrated interdisciplinary research in physics, chemistry, and electronics.[5–9] Promising candidate materials for ReRAM devices are doped perovskite materials such as $SrZrO_3$,[10] ferromagnetic materials such as $(Pr,Ca)MnO_3$ (PCMO),[11] and binary transition-metal oxides such as NiO[12] and TiO_2.[13] Although the switching characteristics have been explained using many models, including the Schottky barrier model,[14] the conductive filamentary model,[8,12,15] the space-charge-limited model,[16] and the metal–insulator transition model,[17] up to now, the driving mechanism of resistive switching is not yet well understood.

ReRAM devices can be classified into two types on the basis of their switching behaviors: unipolar switching and bipolar switching. The polarities of the external voltage for the reset and set processes are identical in unipolar switching,[18] whereas they are opposite in bipolar switching.[19] However, unipolar switching has disadvantages in terms of high operating current and the forming process. Accordingly, bipolar switching may have advantages over unipolar switching in terms of higher uniformity, higher switching speed, and the forming-free process.

Therefore, in this study, we fabricated a bipolar resistive switching memory ($Al/TiO_2/Al$) on a flexible substrate using polyimide, which is well known for its great thermal stability and good chemical resistance. In an earlier work, the substrate was glued onto a Si wafer for mechanical support.[20] However, we do not use a Si-based substrate in this simple fabrication method. In addition, we explain the role of the oxygen vacancies in the TiO_2 layer on the basis of X-ray photoelectron spectroscopy (XPS) and XPS depth profile analysis. Then, good endurance and retention characteristics are examined even at a bending radius of 10 mm. Finally, we demonstrate that the memory performance of a ReRAM on a flexible substrate is excellent compared with previously reported results[20–22] owing to its small channel length and the high ductility of aluminum.

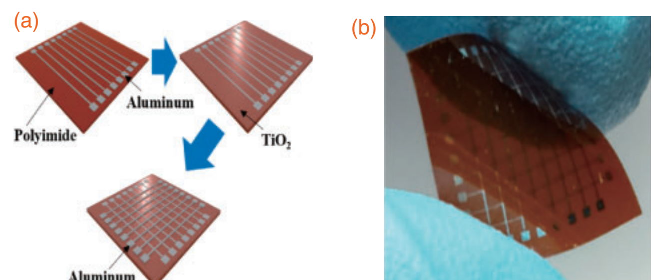

Fig. 1. (a) Schematic image showing the process flow of flexible ReRAM. (b) CCD camera image of the device when device was bent.

A schematic view of our flexible ReRAM on a flexible substrate of polyimide and a bending image of the ReRAM are shown in Fig. 1. Figure 1(a) shows the configuration of a metal–insulator–metal (MIM) structure with a TiO_2 thin film sandwiched between two metal electrodes. Firstly, the bottom electrode was fabricated directly on a flexible substrate of polyimide without a silicon wafer, which would provide mechanical support, by thermal evaporation using a metal shadow mask with eight lines of 60 µm width. Then, a 10-nm-thick TiO_2 thin film was used to form the resistive switching material by atomic layer deposition (ALD). The top aluminum electrode was deposited vertically by thermal evaporation, forming a crossbar-type structure with 8×8 arrays, as shown in Fig. 1(b). The electrical properties (I–V curve) were measured using a Keithley 4200 semiconductor characterization system in the DC voltage sweep mode.

Figure 2(a) shows the typical bipolar I–V characteristics of $Al/TiO_2/Al$ for the 10-nm-thick TiO_2 thin film. Here, voltage bias was applied to the top electrode (TE), while the bottom electrode (BE) was grounded. Before applying the voltage bias, the initial state of the device was the high-resistance state (HRS), and a forming process was not required for this type of resistive switching. The voltage bias was swept in the sequence of $0\,V \rightarrow -3\,V \rightarrow 0\,V \rightarrow 3\,V \rightarrow 0\,V$ under a com-

 © 2014 The Japan Society of Applied Physics

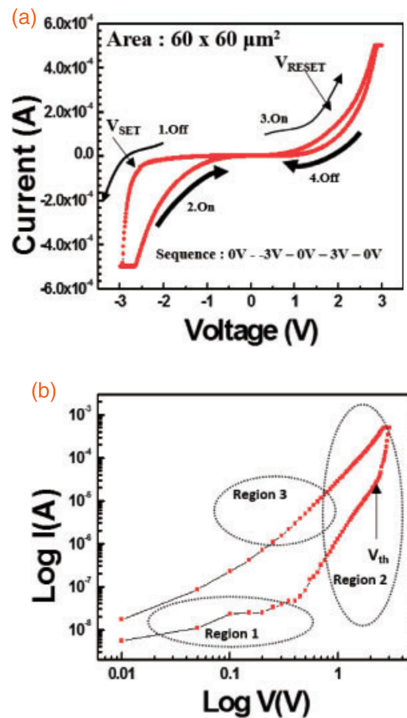

Fig. 2. (a) Typical I–V curve of an $Al/TiO_2/Al$ device on a linear scale. (b) Double logarithmic plot at a negative voltage sweep ($0\,V \rightarrow -3\,V \rightarrow 0\,V$).

pliance current of 500 μA, which was applied to safeguard against device breakdown. The current increased abruptly at a specific negative bias (V_{SET}) and switched from the HRS to the low-resistance state (LRS). The LRS remained during the voltage sweep back to the specific positive bias of less than V_{RESET}. Furthermore, the current decreased abruptly at the specific positive bias (V_{RESET}) and switched from the LRS to the HRS. The resistance ratio (R_{off}/R_{on}) between the HRS and the LRS was greater than 100 at $V_{READ} = -0.4\,V$.

To understand the resistive switching of the $Al/TiO_2/Al$ ReRAM, the I–V curves in the negative-voltage region were replotted using a log–log scale in order to reveal the power relation ($I \propto V$), as can be seen in Fig. 2(b). In the low-voltage region (Region 1), the current was linearly proportional to the voltage ($I \propto V$ for voltages lower than 0.65 V), which corresponds to ohmic behavior. In the intermediate-voltage region (Region 2), the current clearly exhibited Child's law behavior ($I \propto V^2$ for 0.65–1.3 V), and was followed by an exponentially increasing current region ($I \propto V^n$ for 1.3 V). This is the well-known typical trap-associated space-charge-limited current (SCLC) model.[16] Therefore, we believe that the switching phenomenon of the TiO_2-based ReRAM is closely related to the electron trapping and tunneling processes by oxygen vacancies. It was verified that the bipolar resistive switching of $Al/TiO_2/Al$ might originate from the newly generated top interface TiO_x layer. In the TiO_x layer, oxygen ion defects (typically oxygen vacancies) act as traps for electrons injected from the cathode.[23,24]

To probe the existence of the oxygen vacancies, XPS was performed, as shown in Figs. 3(a) and 3(b). The binding energies observed for Ti $2p_{3/2}$ and $2p_{1/2}$ were at 459.3 and 465.3 eV, respectively, which were typically observed in the XPS spectra of Ti^{4+} in TiO_2 showing no trace of Ti^{3+} or Ti^{2+},

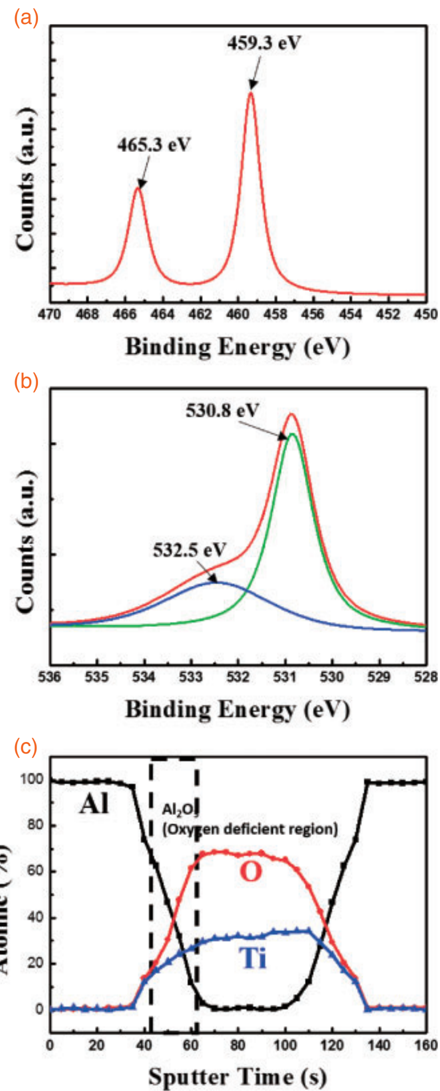

Fig. 3. (a) Ti 2p and (b) O 1s spectra of TiO_2. (c) XPS depth profile analysis of $Al/TiO_2/Al$ device.

whose Ti $2p_{3/2}$ is located at 457.6 and 456.4 eV.[25] Concerning the O 1s spectrum, it can be fitted by Gaussian components at 530.8 and 532.5 eV. The binding energy at 530.8 eV can be assigned to oxygen bound to Ti^{4+} ions in TiO_2, while that at 532.5 eV can be attributed to oxygen deficiencies of TiO_2. A number of studies revealed that nonlattice oxygen is related to the formation of oxygen vacancies.[26] This seems obvious from the XPS analysis results indicating that there are local oxygen vacancies in the TiO_2 layer. Furthermore, to identify the TiO_x layer, XPS depth profile analysis was performed, as shown in Fig. 3(c). After the deposition of the TiO_2 layer, it was significantly changed owing to the reaction with the top Al layer during the deposition process. Commonly, Al is well known as an extremely oxidizable metal. Therefore, Al atoms readily attract oxygen atoms from the TiO_2 layer and react with them, forming an interfacial Al_2O_3 layer.[27] Because of this insulating layer, there is no additional out-diffusion of oxygen ions within the titanium oxide layer, resulting in an oxygen-deficient domain (TiO_x layer) near the top electrode region.[28]

Therefore, the resistive switching phenomenon can be presumed to be due to the oxygen vacancies in the TiO_x layer

© 2014 The Japan Society of Applied Physics

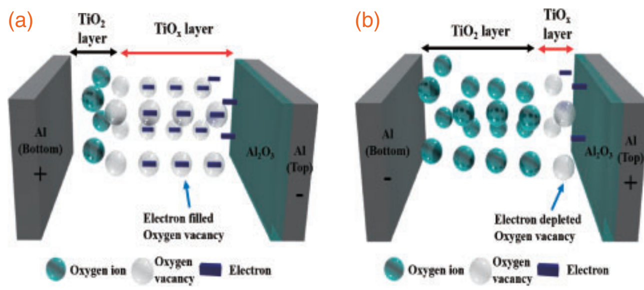

Fig. 4. Schematic diagram of the resistive switching of ReRAM: (a) set and (b) reset processes.

near the top electrode that act as traps for injected electrons, as shown in Fig. 4. During the set process, as shown in Fig. 4(a), the reduction of the Al top electrode occurs owing to the absorption of the oxygen ions in the TiO_2 layers when a negative voltage bias is applied to the top electrode; thereafter, oxygen ions move to the bottom electrode, leaving additional oxygen vacancies in the TiO_x layer. At the bottom electrode, this may lead to the evolution of oxygen gas.[29] The formation of oxygen vacancies can be described in the Kroger–Vink notation as

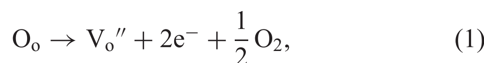

$$O_o \rightarrow V_o'' + 2e^- + \frac{1}{2}O_2, \qquad (1)$$

where V_o'' denotes an oxygen vacancy with a double positive charge with respect to the regular lattice, and O_o represents an oxygen ion on a regular site according to the Kroger–Vink notation. Injected electrons from the top electrode may be captured by a neighboring Ti ion so that the Ti ions may be reduced as

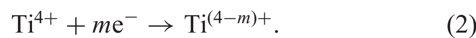

$$Ti^{4+} + me^- \rightarrow Ti^{(4-m)+}. \qquad (2)$$

Because the conduction and valence bands of TiO_x mainly have Ti 3d and O 2p orbital characteristics, respectively, the reduction in the Ti ion concentration means an increase in the free electron population in TiO_x, whereby the reduced Ti ions and the oxygen vacancies can form a metallic phase.[18,30] Therefore, more free electrons in the TiO_x layer result in more electron-filled oxygen vacancies. The electron-filled oxygen vacancies of the so-called "virtual cathode" move towards the bottom electrode, creating a conductive path.[6,9,30] On the other hand, in the case of the reset process shown in Fig. 4(b), oxygen ions diffuse from the TiO_2 layer and oxidize the top electrode when a positive voltage bias is applied to the top electrode. Thereafter, electrons escape from some oxygen vacancies (especially near the top electrode), and electron-depleted oxygen vacancies are recombined with diffused O^{2-} from the TiO_2 layer. This electrochemical process turns a conducting film into an insulating film. For this reason, the resistive switching phenomenon in ReRAM occurs.

Next, to examine the nonvolatile ReRAM characteristics of our flexible devices, endurance and retention measurements were obtained at room temperature. Figure 5(a) shows the endurance test results (write–read–erase–read cycles) of the $Al/TiO_2/Al$ resistive switching memory cell. The reading voltage pulse was −0.4 V after both the set process (−3 V, 1 µs) and the reset process (+3 V, 1 µs). The resistances of both states were distributed in certain voltage regions, especially for

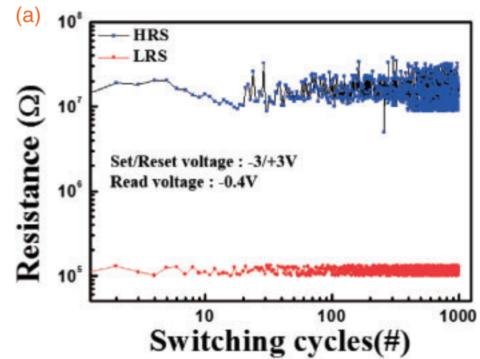

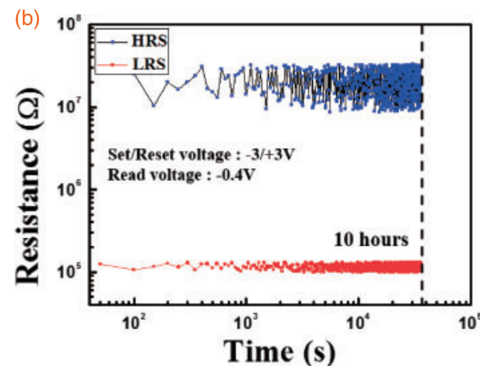

Fig. 5. (a) Endurance characteristics of the $Al/TiO_2/Al$ device under the current compliance of 500 µA (write–read–erase–read sequence). (b) Retention characteristics of the $Al/TiO_2/Al$ device over a period of 10 h. The reading voltage was maintained at −0.4 V.

the HRS. However, with a sufficient energy to extinguish the R_{off}/R_{on} ratio gap, the resistive switching memory cell exhibits tolerance to this type of scattering. As can be seen, the memory gap was beyond the R_{off}/R_{on} ratio of 100 during 10^3 cycles. The endurance measurements demonstrate that the switching between the ON and OFF states is highly reversible and reproducible. After the device was switched ON or OFF, no additional electrical power was needed to maintain the resistance in a given state. The retention characteristic of the fabricated resistive switching memory cell was determined, and the obtained results are shown in Fig. 5(b). The current was read at a bias of −0.4 V every 50 s after the set (−3 V) and reset (3 V) processes. No critical changes in resistance in either case were observed for 10 h, whereas a sufficient gap in the resistance ratio was observed for over 10^4 s. This indicates the feasibility of nonvolatile application of the device.

A mechanical bending test of the ReRAM on a flexible substrate was performed to determine whether the mechanical flexibility would be sufficient for flexible memory applications. Figure 6(a) shows the bending test results as a function of bending radius. In the test, the bending radius was varied from 100 to 10 mm, and the results showed that severe bending of the ReRAM did not affect the device characteristics. In addition, retention and endurance [Figs. 6(b) and 6(c)] were examined at the bending radius of 10 mm, and their values were observed to be similar to those in Figs. 5(b) and 5(c). Accordingly, the device exhibited a good resistance ratio owing to the good ductility of aluminum and the small channel length.

In this work, we successfully demonstrated flexible ReRAM ($Al/TiO_2/Al$) devices fabricated by a simple method

© 2014 The Japan Society of Applied Physics

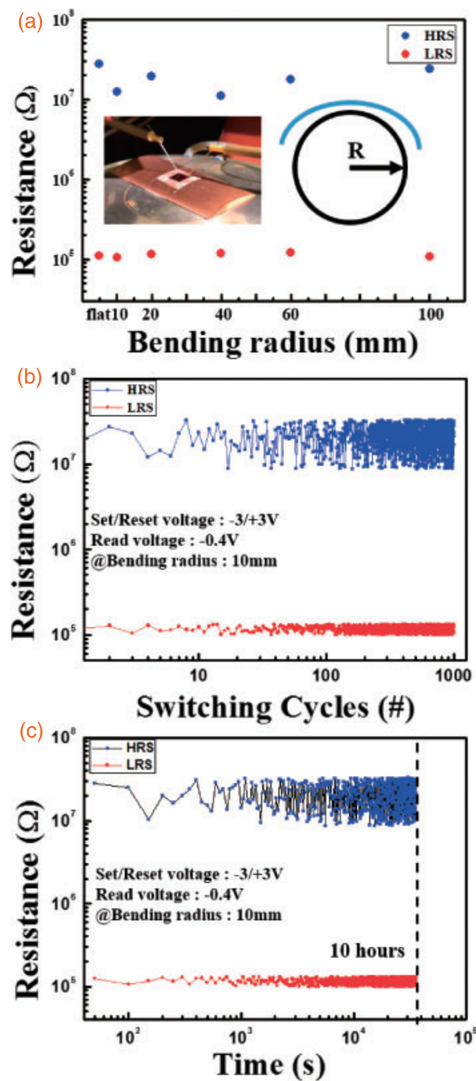

Fig. 6. Flexibility test results. (a) All data were measured from six different radii. The reading voltage was −0.4 V. The inset shows the device on the bending substrate. (b) Endurance. (c) Retention.

on a polyimide substrate rather than on a Si-based substrate. The resistive switching phenomenon was clearly explained by XPS analysis showing the existence of oxygen vacancies. XPS depth profile analysis showed that the resistive switching phenomenon is generated from TiO_x, which plays an important role in the proposed ReRAM with an $Al/TiO_2/Al$ structure. Moreover, our devices exhibited reliable endurance and retention characteristics, even at a severe bending radius, owing to the high ductility of the aluminum electrode and the small channel length. These results clearly demonstrate that a flexible ReRAM can be expected to enable the development of a broadly applicable emerging memory technology in the semiconductor industry and to play an important role in the dissemination of low-cost, high-performance devices. Our devices indicate the possibility of the emerging memory as a promising technique for flexible devices.

Acknowledgments This research was supported by the KSSRC Program (External Mechanical Stress on MOSFET). This work was also supported by the Industrial Strategic Technology Development Program (10045269, Development of Soluble TFT and Pixel Formation Materials/Process Technologies for AMOLED TV) funded by MOTIE/KEIT and partially supported by the National Research Foundation of Korea (NRF) grant funded by the Korea government (MSIP) (CAFDC 4-2, NRF-2007-0056090).

1) S. Ju, A. Facchetti, Y. Xuan, J. Liu, F. Ishikawa, P. Ye, C. Zhou, T. J. Marks, and D. B. Janes, Nat. Nanotechnol. **2**, 378 (2007).
2) Y. Chen, J. Au, P. Kazlas, A. Ritenour, H. Gates, and M. McCreary, Nature **423**, 136 (2003).
3) M. C. McAlpine, H. Ahmad, D. Wang, and J. R. Heath, Nat. Mater. **6**, 379 (2007).
4) R. H. Reuss, B. R. Chalamala, A. Moussessian, M. G. Kane, A. Kumar, D. C. Zhang, J. A. Rogers, M. Hatalis, D. Temple, G. Moddel, B. J. Eliasson, M. J. Estes, J. Kunze, E. S. Handy, E. S. Harmon, D. B. Salzman, J. M. Woodall, M. A. Alam, J. Y. Murthy, S. C. Jacobsen, M. Olivier, D. Markus, P. M. Campbell, and E. Snow, Proc. IEEE **93**, 1239 (2005).
5) G. I. Meijer, Science **319**, 1625 (2008).
6) R. Waser, R. Dittmann, G. Staikov, and K. Szot, Adv. Mater. **21**, 2632 (2009).
7) A. Sawa, Mater. Today **11** [6], 28 (2008).
8) K. Szot, R. Dittmann, W. Speier, and R. Waser, Phys. Status Solidi: Rapid Res. Lett. **1**, R86 (2007).
9) R. Waser and M. Aono, Nat. Mater. **6**, 833 (2007).
10) A. Beck, J. G. Bednorz, C. Gerber, C. Rossel, and D. Widmer, Appl. Phys. Lett. **77**, 139 (2000).
11) S. Md. Sadaf, E. M. Bourim, X. Liu, S. H. Choudhury, D.-W. Kim, and H. Hwang, Appl. Phys. Lett. **100**, 113505 (2012).
12) J.-B. Yun, S. Kim, S. Seo, M.-J. Lee, D.-C. Kim, S.-E. Ahn, Y. Park, J. Kim, and H. Shin, Phys. Status Solidi: Rapid Res. Lett. **1**, 280 (2007).
13) Y. C. Shin, M. H. Lee, K. M. Kim, G. H. Kim, S. J. Song, J. Y. Seok, and C. S. Hwang, Phys. Status Solidi: Rapid Res. Lett. **4**, 112 (2010).
14) S. Park, S. Jung, M. Siddik, M. Jo, J. Park, S. Kim, W. Lee, J. Shin, D. Lee, G. Choi, J. Woo, E. Cha, B. H. Lee, and H. Hwang, Phys. Status Solidi: Rapid Res. Lett. **6**, 454 (2012).
15) H. J. Wang, C. W. Zou, L. Zhou, C. X. Tian, M. K. Lee, J. C. Lee, T. W. Kang, and D. J. Fu, Phys. Status Solidi: Rapid Res. Lett. **5**, 223 (2011).
16) S. Kim, H. Y. Jeong, S.-Y. Choi, and Y.-K. Choi, Appl. Phys. Lett. **97**, 033508 (2010).
17) G. I. Meijer, U. Staub, M. Janousch, S. L. Johnson, B. Delley, and T. Neisius, Phys. Rev. B **72**, 155102 (2005).
18) K. M. Kim, D. S. Jeong, and C. S. Hwang, Nanotechnology **22**, 254002 (2011).
19) K. Oka, T. Yanagida, K. Nagashima, H. Tanaka, and T. Kawai, J. Am. Chem. Soc. **131**, 3434 (2009).
20) S. Kim and Y.-K. Choi, Appl. Phys. Lett. **92**, 223508 (2008).
21) H. Y. Jeong, J. Y. Kim, J. W. Kim, J. O. Hwang, J. E. Kim, J. Y. Lee, T. H. Yoon, B. J. Cho, S. O. Kim, R. S. Ruoff, and S. Y. Choi, Nano Lett. **10**, 4381 (2010).
22) S. Kim, H. Moon, D. Gupta, S. Yoo, and Y.-K. Choi, IEEE Trans. Electron Devices **56**, 696 (2009).
23) S. Kim and Y.-K. Choi, IEEE Trans. Electron Devices **56**, 3049 (2009).
24) S. Kim, O. Yarimaga, S.-J. Choi, and Y.-K. Choi, Solid-State Electron. **54**, 392 (2010).
25) S.-Z. Chen, P.-Y. Zhang, W.-P. Zhu, L. Chen, and S.-M. Xu, Appl. Surf. Sci. **252**, 7532 (2006).
26) Q. Mao, Z. Ji, and J. Xi, J. Phys. D **43**, 395104 (2010).
27) H. Y. Jeong, J. Y. Lee, S.-Y. Choi, and J. W. Kim, Appl. Phys. Lett. **95**, 162108 (2009).
28) H. Y. Jeong, S. K. Kim, J. Y. Lee, and S.-Y. Choi, J. Electrochem. Soc. **158**, H979 (2011).
29) D. S. Jeong, H. Schroeder, U. Breuer, and R. Waser, J. Appl. Phys. **104**, 123716 (2008).
30) M. Janousch, G. I. Meijer, U. Staub, B. Delley, S. F. Karg, and B. P. Andreasson, Adv. Mater. **19**, 2232 (2007).

© 2014 The Japan Society of Applied Physics